

Impacts of
AMSU-A/MHS and
IASI data assimilation

Y. Bao et al.

This discussion paper is/has been under review for the journal Atmospheric Measurement Techniques (AMT). Please refer to the corresponding final paper in AMT if available.

Impacts of AMSU-A/MHS and IASI data assimilation on temperature and humidity forecasts with GSI/WRF over the Western United States

Y. Bao^{1,2}, J. Xu², A. M. Powell Jr.³, and M. Shao²

¹ Collaborative Innovation Center on Forecast and Evaluation of Meteorological Disasters, Key Laboratory for Aerosol-Cloud-Precipitation of China Meteorological Administration, Nanjing University of Information Science and Technology, Nanjing, China

² Global Environment and Natural Resources Institute, College of Science, George Mason University, Fairfax, Virginia, USA

³ NOAA/NESDIS/STAR, College Park, Maryland, USA

Received: 30 April 2015 – Accepted: 5 June 2015 – Published: 25 June 2015

Correspondence to: J. Xu (jxu14@gmu.edu)

Published by Copernicus Publications on behalf of the European Geosciences Union.

Title Page

Abstract

Introduction

Conclusions

References

Tables

Figures



Back

Close

Full Screen / Esc

Printer-friendly Version

Interactive Discussion



Abstract

Using NOAA's Gridpoint Statistical Interpolation (GSI) data assimilation system and NCAR's Advanced Research WRF (ARW-WRF) regional model, six experiments are designed by (1) control experiment (CTRL) and five data assimilation (DA) experiments with different data sets including (2) conventional data only (CON), (3) microwave data (AMSU-A + MHS) only (MW), (4) infrared data (IASI) only (IR), (5) combination of microwave and infrared data (MWIR), (6) combination of conventional, microwave and infrared observation data (ALL). One month experiments in July 2012 and impacts of the DA on temperature and moisture forecasts at the surface and four vertical layers, which over the western United States have been investigated. The four layers include lower troposphere (LT) from 800 to 1000 hPa, middle troposphere (MT) from 400 to 800 hPa, upper troposphere (UT) from 200 to 400 hPa and lower stratosphere (LS) from 50 to 200 hPa. The results show that the regional GSI/WRF system is underestimating the observed temperature in the LT and overestimating in the UT and LS. The MW DA reduced the forecast bias from the MT to the LS within 30 h forecasts, and the CON DA kept a smaller forecast bias in the LT for 2-day forecasts. The largest RMS error is observed in the LT and at the surface (SFC). Compared to the CTRL, the MW DA made the most positive contribution in the UT and LS, and the CON DA mainly improved the temperature forecasts at the SFC. However, the IR DA made a negative contribution in the LT.

Most of the observed humidity in the different vertical layers is overestimated in the humidity forecasts except in the UT. The smallest bias in the humidity forecast occurred at the SFC and UT. The DA experiments apparently reduced the bias from the LT to UT, especially for the IR DA experiment, but the RMS errors are not reduced in the humidity forecasts. Compared to the CTRL, the IR DA experiment has a larger RMS error in the moisture forecast although the smallest bias is found in the LT and MT.

AMTD

8, 6439–6467, 2015

Impacts of AMSU-A/MHS and IASI data assimilation

Y. Bao et al.

Title Page

Abstract

Introduction

Conclusions

References

Tables

Figures



Back

Close

Full Screen / Esc

Printer-friendly Version

Interactive Discussion



1 Introduction

Instead of a random distribution and heterogeneous spatial density in the traditional radiosondes, satellite observations provide a large amount of data covering worldwide areas for improving the initialization of the weather forecasts models through a data assimilation system. Many studies demonstrated that the assimilation of satellite data significantly improved weather forecasts (Eyre 1992; Andersson et al., 1991; Derber and Wu 1998; Zhou et al., 2011), especially over some areas with sparse conventional observations (McNally et al., 2000; Zapotocny et al., 2008; Liu et al., 2012).

The Meteorological Operational satellite program (MetOp) launched its first polar orbiting satellite (MetOp-A) on 19 October 2006. MetOp-A is in a sun-synchronous orbit, carrying a payload of 10 scientific instruments including the Advanced Microwave Sounding Unit- A (AMSU-A), Microwave Humidity Sounder (MHS) and the new generation Infrared Atmospheric Sounding Interferometer (IASI) to make atmospheric soundings at various altitudes. IASI (Clerbaux et al., 2009) measures the radiance emitted from the Earth in 8461 channels covering the spectral interval 645–2760 cm^{-1} at a resolution of 0.5 cm^{-1} (apodized) and with a spatial sampling of 18 km at nadir. Limited spectral data is currently transmitted, stored and assimilated. Rabier et al. (2002) compared a number of techniques for channel selection from high-spectral-resolution infrared sounders, and concluded that the channel-selection method of Rodgers (1996, 2000) is the most optimal. Collard (2007) applied his method to select a subset of 300 channels for data assimilation, so that the total loss of information for a typical numerical weather prediction (NWP) state vector consisting of one or more of temperature, humidity is minimized.

This study focuses on assessing effects of AMSU-A, MHS and IASI data assimilation on numerical weather forecasts over the western United States. The model, data and methodology are presented in the Sects. 2 and 3, respectively. Section 4 describes the results of experiments. The results are summarized and discussed in Sect. 5.

AMTD

8, 6439–6467, 2015

Impacts of AMSU-A/MHS and IASI data assimilation

Y. Bao et al.

Title Page

Abstract

Introduction

Conclusions

References

Tables

Figures



Back

Close

Full Screen / Esc

Printer-friendly Version

Interactive Discussion



2 Model

2.1 The GSI system for ARW WRF regional model

The assimilation system used here is the Gridpoint Statistical Interpolation (GSI) analysis system, which is developed by United States National Centers for Environmental Prediction (NCEP). The current GSI regional analysis system accepts NCEP's Nonhydrostatic Mesoscale Model (NMM) WRF and NCAR's Advanced Research WRF (ARW) WRF mass core (Liu and Weng, 2006a; Xu and Powell, 2012; Wan and Xu, 2011). Interface is specialized separately for the WRF NMM core and the WRF ARW core. The analysis system produces an analysis through the minimization of an objective function given by

$$J = \frac{1}{2}(x - x^b)^T B^{-1}(x - x^b) + \frac{1}{2}(H(x) - y^o)^T R^{-1}(H(x) - y^o)$$

Where x is the analysis state, B is the background error covariance matrix, x^b is the first guess that is from GFS 6 h forecast filed in this study, H is the transformation operator from the analysis variable to the form of the observations, y^o is the observation such as AMSU-A, MHS, IASI, etc.

The minimization algorithm is composed of two outer iterations to account for weak nonlinearities in the cost function. In the first external iteration the first guess is a 6 h forecast, while in the second one it is the solution from the previous outer iteration. In the cost function, B has been estimated from scaled differences between 24 and 48 h forecasts valid at the same time (Parrish and Derber, 1992). The observation error covariance matrix (R) contain information on the observational error and errors in representativeness, which has been calculated before running the GSI.

Impacts of AMSU-A/MHS and IASI data assimilation

Y. Bao et al.

Title Page

Abstract

Introduction

Conclusions

References

Tables

Figures



Back

Close

Full Screen / Esc

Printer-friendly Version

Interactive Discussion



2.2 Radiative Transfer Model

The radiative transfer model incorporated into the GSI data assimilation system at the NCEP is the Community Radiative Transfer Model (CRTM). The CRTM was developed by the U.S. Joint Center for Satellite Data Assimilation (JCSDA) for rapid calculations of satellite radiances based on radiative transfer (RT) theory (Han et al., 2006). The forward model, tangent-linear, adjoint and K-matrix models were also developed for data assimilation of satellite data. CRTM is always updated for new satellite data. It supports a large number of sensors onboard geostationary and polar-orbiting satellites, covering the microwave, infrared and visible frequency regions.

The CRTM comprises four major modules: (1) RT solution module, (2) atmospheric transmittance module, (3) surface emissivity/reflectivity module, (4) particle scattering module. Six RT solution schemes were tested in the CRTM (Weng et al., 2007). According to several performance factors, the advance doubling and adding scheme (ADA; Liu and Weng, 2006b) was selected for the CRTM implementation. In CRTM, a fast and optimal spectral sampling (OSS) absorption model (Moncet et al., 2004) is used to calculate atmospheric transmittance.

2.3 Experiment design

The objective of this study is to explore the effect of satellite data assimilation on the main atmospheric state forecast through comparing the results from microwave (AMSU-A and MHS), hyperspectral infrared radiance (IASI) and conventional data assimilation. Over the main continent of United States of America (USA), there are many conventional observation stations, which can be used to validate the forecast results. Therefore, the western coast region of the USA is selected to the experimental region. Analyzing the satellite data (AMSU-A, MHS and IASI) covering the western USA at 00:00, 06:00, 12:00 and 18:00 UTC, the satellite data at 18:00 UTC covered more of the region than at other anytime. The covered region at 18:00 UTC is 20–55° N and 85–155° W, which includes the western USA and sea area near the west coast (Fig. 1).

Impacts of AMSU-A/MHS and IASI data assimilation

Y. Bao et al.

Title Page

Abstract

Introduction

Conclusions

References

Tables

Figures



Back

Close

Full Screen / Esc

Printer-friendly Version

Interactive Discussion



**Impacts of
AMSU-A/MHS and
IASI data assimilation**

Y. Bao et al.

Title Page

Abstract

Introduction

Conclusions

References

Tables

Figures



Back

Close

Full Screen / Esc

Printer-friendly Version

Interactive Discussion



The experiment design includes six simulations (Table 1). The control (CTRL) experiment is first made with an initial time at 18:00 UTC and makes 6 h forecasts. The five data assimilation (DA) experiments and the second control experiment are made with initial time at 00:00 UTC from 1 to 31 July 2012 and make a 72 h forecast for each day. The initial condition in all six experiments is obtained from the 6 h forecasts of the first control experiment. The five DA experiments are made with different data sets including conventional data only (CON), microwave data (AMSU-A + MHS) only (MW), infrared data (IASI) only (IR), a combination of microwave and infrared data (MWIR), a combination of conventional, microwave and infrared observation data (ALL). The initial condition and lateral boundary conditions came from the operational GFS forecast at 6 h intervals and $0.5^{\circ} \times 0.5^{\circ}$ resolution, which were downloaded from NCEP data inventory (<ftp://ftp.ncep.noaa.gov/pub/data/nccf/com/gfs/prod/>).

In the ARW model, the physics of the model includes the Goddard Cumulus Ensemble (GCE) microphysics scheme, Yosei University planetary boundary layer (PBL) scheme, Noah land surface model, Rapid Radiative Transfer Model (RRTM) longwave radiation, and the Goddard shortwave radiation scheme. The 15 km WRF model forecast with a mesh size domain of 718×373 (Fig. 1) was used. Forty-three (43) vertical layers were selected for use with a model top of 10 Pa.

3 Data and methodology

3.1 Conventional and satellite data

In this study, the conventional observation data includes atmospheric temperature (T), moisture (Q) and wind speed (WSP) at various pressure levels and pressure data at the surface. Figure 1a shows the distribution of the conventional data on 1 July 2012 where the atmospheric temperature, moisture and surface pressure observations are rare. Most atmospheric temperature and moisture observations are conducted at the

surface level in pressure range of 1000–1200 hPa. The most WSP data are found over the sea close to the coast of western United States.

The satellite data includes the Advanced Microwave Sounding Unit-A (AMSU-A), Microwave Humidity Sounder (MHS) and the new generation Infrared Atmospheric Sounding Interferometer (IASI). Figure 1b shows the distribution of the AMSU-A, MHS and IASI datasets. AMSU-A is a 15-channel cross-track, stepped-line scanning, total power microwave radiometer. The channels from 4 to 14 are assimilated in this study, which were designed to detect atmospheric temperature at 11 layers from the surface to around 45 km. Their weighting function is illustrated by Fig. 2a. MHS on the other hand probes at millimetric frequencies between 89 and 183 GHz, the channels from 2 to 5 are assimilated, which were designed to detect atmospheric moisture at 2 layers from surface to around 400 hPa. Their weighting function is illustrated by Fig. 2b. Channel 4 of AMSU-A and channel 2 of MHS can detect the atmospheric temperature and humidity at the lowest layer of the troposphere. Channels 5 and 6 of AMSU-A and channels 3, 4 and 5 of MHS can detect the atmospheric temperature and humidity in the middle atmospheric layer of the troposphere. Channel 7 of AMSU-A can detect the atmospheric temperature in the highest layer of troposphere. Channels 9 and 10 of AMSU-A can detect the atmospheric temperature in lower layer of the stratosphere.

The IASI instrument covers the spectral range from the thermal infrared at $3.62\ \mu\text{m}$ ($2760\ \text{cm}^{-1}$) to $15.5\ \mu\text{m}$ ($645\ \text{cm}^{-1}$) covering the peak of the thermal infrared and particularly the CO_2 band with the humidity (Q) branch around $666\ \text{cm}^{-1}$. Within these bands, the selected 279 bands (Table 2) correspond to atmospheric temperature and humidity. A band number smaller than 515 represents atmospheric temperature, and a band number larger than 2701 represents atmospheric humidity. Their weighting function is illustrated by Fig. 2c.

3.2 Radiance data quality control and bias correction

The radiance data have been preprocessed by NESDIS before becoming available for usage. The data have been statistically limb corrected (adjusted to nadir) and surface

Impacts of AMSU-A/MHS and IASI data assimilation

Y. Bao et al.

Title Page

Abstract

Introduction

Conclusions

References

Tables

Figures



Back

Close

Full Screen / Esc

Printer-friendly Version

Interactive Discussion



Impacts of AMSU-A/MHS and IASI data assimilation

Y. Bao et al.

Title Page

Abstract

Introduction

Conclusions

References

Tables

Figures

◀

▶

◀

▶

Back

Close

Full Screen / Esc

Printer-friendly Version

Interactive Discussion



emissivity corrected in the microwave channels and cloud cleared in the tropospheric channels. Although the satellite data have undergone preprocessing, they need further bias correction before being ingested in data assimilation system. The source of the biases can be related to instrument calibration problems, and predictor and zenith angle bias. It was demonstrated that a successful bias correction scheme must take into account the spatially varying and air-mass dependent nature of radiance biases. Previous publications have (Kelly and Flobert, 1988; McMillin et al., 1989; Udchrtrom, 1991). Eyre (1992) and Harris and Kelly (2001) categorized the bias into two types: scan bias and air-mass bias, and presented a bias correction scheme. GSI uses this bias correction scheme to correct radiance bias. The radiance bias correction coefficients might be downloaded from GDAS (define GDAS) data directory, and be used to correct the radiance bias in GSI. To that purpose, monthly regional mean innovations, e.g. observation minus background (OMB) and observation minus analysis (OMA), are calculated with or without bias corrections in this study. For example, Fig. 3 is the scattering plots of surface pressure, atmospheric temperature at the height of 2 m and wind speed at the height of 10 m between OMB and OMA in the ALL data experiment. The result shows that the slope of the simulated line is less than 1, which indicates the analysis fields are closer to observation than background fields.

3.3 Methodology

In order to evaluate the effects of radiance data assimilation on temperature and moisture at the different vertical layers, the surface (SFC) and four atmospheric layers are examined. The four layers include lower troposphere (LT) from 800 to 1000 hPa, middle troposphere (MT) from 400 to 800 hPa, upper troposphere (UT) from 200 to 400 hPa and lower stratosphere (LS) from 50 to 200 hPa. Similar to the previous study (Xu et al., 2009), two statistical variables – bias and root mean square (RMS) error are investigated.

If X represents any of the parameters under consideration for a given time and vertical level, then forecast error is defined as $X' = X_f - X_o$ where the subscripts f and o

denote forecast and observed quantities, respectively. Given N valid pairs of forecasts and observations, the bias is computed as

$$\text{bias} = \overline{X'} = \frac{1}{N} \sum_{i=1}^N X'_i \quad (1)$$

the root mean-square (RMS) error is computed as

$$\text{RMS} = \sqrt{\frac{1}{N} \sum_{i=1}^N (X'_i)^2} \quad (2)$$

The bias and RMS error at 00:00 and 12:00 UTC are calculated because more than enough observational data and approximately 3000 sounding stations can be used at the two times.

4 Results

4.1 Temperature

At the SFC, the CON (conventional data only) DA experiment shows (Fig. 4a) the smallest bias value in all six experiments. Three involved infrared satellite DA experiments (IR, IR + MW, IR + MW + CON) showing a larger bias than the CTRL experiment. It seems that satellite radiance DA, especially for the infrared IASI data, make a negative contribution to the temperature forecasts. Interestingly, the bias characterized a diurnal cycle feature for the 72 h forecasts, with the smaller bias appearing at 06, 30, 54 and 72 h corresponding to a local time at 4:00 p.m. while the higher bias appeared at 18, 42 and 66 h corresponding to 4:00 a.m. local time.

Compared to the SFC, the LT shows a more clear diurnal variation (Fig. 4b), and all model forecasts underestimated the observed temperature. The CTRL and CON experiments obtained the smallest forecast bias.

Impacts of AMSU-A/MHS and IASI data assimilation

Y. Bao et al.

Title Page

Abstract

Introduction

Conclusions

References

Tables

Figures

◀

▶

◀

▶

Back

Close

Full Screen / Esc

Printer-friendly Version

Interactive Discussion



Impacts of AMSU-A/MHS and IASI data assimilation

Y. Bao et al.

Title Page

Abstract

Introduction

Conclusions

References

Tables

Figures



Back

Close

Full Screen / Esc

Printer-friendly Version

Interactive Discussion



Different from the SFC and LT, the diurnal variation of bias disappeared in the MT (Fig. 4c). Compared to the CTRL experiment, the bias is significantly reduced in all DA experiments especially for the two combination experiment (MWRI and ALL), the bias is almost zero with the 30 h forecast. It implies that both MW (AMUS-A and MHS) and IR (IASI) DA make a positive contribution to the accuracy of temperature forecasts at the MT.

At the UT, the smaller bias appeared at the CON and MW DA experiments (Fig. 4d), and the combination DA experiments (MWIR and ALL) show a larger bias than the CTRL experiment. The results indicate that the IR DA made a negative contribution to the temperature forecasts and the MW experiment improved the forecast accuracy in the UT.

In contrast, the bias in the LS indicates an opposite pattern to the SFC and LT that all satellite DA experiments reduced the forecast bias (Fig. 4e). The result demonstrated that the conventional DA did not improve the forecasts because of the rare observational data used in this layer. The MW DA obtained the smallest bias at the LS.

In order to clearly understand the different performance in the six experiments, the temperature forecast bias profile at 6, 30 and 54 h has been examined. Figure 5 indicates a similar pattern at the three forecast times where the lower bias can be found at the SFC and MT while the larger bias appeared at the UT and LS. Generally, the model forecasts overestimated the observed temperature except in the LT. Compared to the CTRL experiment, the four satellite DA experiments (MW, IR, MWIR and ALL) show a smaller bias from the MT through LS, but the forecasts did not get improved in the LT below 800 hPa. In contrast, the CON experiment has better performance in the LT, especially at the SFC.

It is obvious that the larger bias in temperature forecast appeared in the LT, UT and LS, but the model is underestimating the observed temperature in the LT and overestimating in the UT and LS (Fig. 5). The satellite DA, especially for the MW DA experiment using AMSU-A, reduced the forecast bias at the level from the MT to LS.

Meanwhile, the CON DA has a smaller forecast bias in the LT, especially at the SFC. Note the IR experiment using the IASI data produced a worst result in the LT.

The forecast RMS error demonstrated some different features (Fig. 6). First, the RMS error reduced the diurnal variation and the RMS error significantly increased with the extended length of forecast time at the SFC. The RMS error in the CON and MW experiments is slightly less than that in the CTRL experiment and the other three satellite DA experiments within 24 h forecasts (Fig. 6a). Second, consistent with the larger negative bias in all the satellite DA experiments (Fig. 4b) in the LT, larger RMS errors are observed in these DA experiments (Fig. 6b) compared to the CTRL. Third, different from the smaller bias in the DA experiments, the larger RMS errors are maintained in the DA experiments in the MT (Fig. 6c). Forth, the CON and MW experiments improved the temperature forecasts in the UT (Fig. 6d). But in the LS, the involved microwave DA experiments including MW, MWIR and ALL indicate the smaller RMS errors than the CTRL experiments (Fig. 6e). It is apparent that the CON DA made a negative contribution to the temperature forecast in the LS.

Corresponding to the bias profile (Fig. 5), the forecast RMS error profile at 6, 30 and 54 h indicates (Fig. 7) that the smallest RMS error is observed at the MT and the largest RMS error appeared in the LT and SFC. Compared to the CTRL experiment, the smaller RMS errors are only found in the MW experiment in the UT and LS, and the CON DA made a positive contribution at the SFC and UT.

The results clearly show the IR DA experiment makes a negative contribution to the temperature forecast in the regional system. But the MW DA experiment shows a positive contribution at the LS, and the CON experiment displays better performance at the SFC and UT. It is worth noticing that the RMS error is not always consistent with the bias in the temperature forecasts, for example, the smaller bias appeared at the SFC while a larger RMS error is observed there.

AMTD

8, 6439–6467, 2015

Impacts of AMSU-A/MHS and IASI data assimilation

Y. Bao et al.

Title Page

Abstract

Introduction

Conclusions

References

Tables

Figures



Back

Close

Full Screen / Esc

Printer-friendly Version

Interactive Discussion



4.2 Humidity

Similar to the temperature forecasts at the SFC, the diurnal variation of the moisture bias is observed and the smallest bias appeared in the CON and CTRL experiments within the 42 h forecast (Fig. 8a) with largest bias occurring in the MWIR experiment at 18 h. It is clear that all four satellite DA experiments do not improve the moisture forecast compared to the CTRL experiment. In contrast, the IR DA produced a larger bias significantly differing from the other experiments in entire troposphere (Fig. 8b–d). It seems to tell us that the IR DA significantly impacts the humidity forecasts in the troposphere. However, the impacts disappeared in the LS (Fig. 8e).

Compared to the bias profile of the temperature forecast (Fig. 4), all model runs over-estimated the observed humidity except for the UT. The smallest bias in the humidity forecast occurred at the SFC and UT (Fig. 9). Most of DA experiments apparently reduced the bias from LT to UT, especially for the IR experiment. But it is worth noting that the MW DA has a larger bias than the CTRL experiment in the whole troposphere.

However, the RMS error in the humidity forecasts (Fig. 10) increases from the SFC to LS. The largest error in the UT and LS is almost double the amount at the SFC. In addition, most of DA experiments demonstrated a larger RMS error than that in the CTRL experiment. In other words, the DA experiments made a negative contribution to the humidity forecasts. The IR DA experiment did not improve moisture forecast although its bias is very small at the LT and MT.

5 Summary and discussion

5.1 Summary

In this study, six experiments were designed to assess the effects of data assimilation on atmospheric temperature and moisture forecasts over the western United States. The results are summarized as follows.

Impacts of AMSU-A/MHS and IASI data assimilation

Y. Bao et al.

Title Page

Abstract

Introduction

Conclusions

References

Tables

Figures



Back

Close

Full Screen / Esc

Printer-friendly Version

Interactive Discussion



Impacts of AMSU-A/MHS and IASI data assimilation

Y. Bao et al.

Title Page

Abstract

Introduction

Conclusions

References

Tables

Figures



Back

Close

Full Screen / Esc

Printer-friendly Version

Interactive Discussion



The regional model underestimates the observed temperature in the LT and overestimates it in the UT and LS. The MW experiment reduced the forecast bias from the MT to LS, and the CON DA obtained a smaller forecast bias in the LT, especially at the SFC. But the IR experiment using the IASI data obtained the largest bias in the LT.

However, the RMS error is not always consistent with the bias profile in the temperature forecasts, the RMS error profile shows that the largest RMS error appeared in the LT and the smallest error in the MT. Compared to the CTRL experiment, the smaller RMS errors are only found in the MW experiment in the UT and LS, and the CON DA made a positive contribution at the SFC and in the UT. The IASI DA experiment made a negative contribution to the temperature forecast in the regional forecast system.

In contrast, all model forecasts overestimated the observed humidity except in the UT. The smallest bias in the humidity forecast occurred at the SFC and in the UT. Most of DA experiments apparently reduced the bias in the LT to UT, especially for the IR DA experiment. But the MW DA obtained a larger bias than the CTRL experiment in the entire troposphere.

The RMS error in the humidity forecasts increases from the SFC to the LS, which is similar to the bias profile except in the UT. The largest error in the UT and LS is almost double the amount at the SFC. The DA experiments make a limited contribution to the humidity forecasts. The IR DA experiment does not improve the moisture forecast although its smallest bias is found in the LT and MT.

5.2 Discussion

This is a study using WRF-ARW mesoscale model linkage with GSI data assimilation system to explore the impacts of AMSU-A/MHS and IASI radiance data assimilation on the temperature and humidity forecasts in the different vertical layers over the western coast of United States, due to the complexity of measurements for satellite instruments (such as IASI has 8461 channels) and lack of knowledge in the estimation of impacts of those dataset in this regional area, forecasters should be aware of the limitations of these data assimilation when forecasting in this region.

Impacts of AMSU-AMHS and IASI data assimilation

Y. Bao et al.

Title Page

Abstract

Introduction

Conclusions

References

Tables

Figures



Back

Close

Full Screen / Esc

Printer-friendly Version

Interactive Discussion



The results show that the bias and forecast error is substantially related to the vertical layer of the objective. For example, the AMSU-A data assimilation reduced the temperature forecast bias in the upper atmospheric layers, the conventional data assimilation indicates the best performance in the lower layer, but the IASI data assimilation shows worst performance in the lower layer. Compared to the largest bias in the upper atmospheric layer, the largest RMS error appeared in the lower atmospheric layers. The humidity forecast is different, the IASI data assimilation significantly reduced the bias in the troposphere, but the RMS error tells us that the IASI data assimilation does not improve the moisture forecast in this layer. The reason is very complicated, it is partially attributed to the data selection in the processes of the data assimilation. The results shown in this analysis demonstrate the some impacts of satellite data on temperature and humidity forecasts in this region, but the positive or negative impact depends on the atmospheric layer and forecasts variables.

It is worth noting that the results presented here are based on one month's forecasts with three satellite instruments. The model performance needs to be examined with longer experiments and more data selection that extend to all available satellite data sets and more experiments from the different areas. As expressed by Manning and Davis (1997), "These statistics would provide additional information to model users and alert model developers to those research areas that need more attention."

Acknowledgements. The GSI data assimilation system was obtained from Joint Center for Satellite Data Assimilation (JCSDA), WRF-ARW model was obtained from the NCAR, the satellite datasets were provided by NOAA/NESDIS/STAR. The authors would like to thank these agencies for the model and data providing. This work was partially supported by a project funded by the Priority Academic Program Development of Jiangsu Higher Education Institutions (PAPD), the Major State Basic Research Development Program of China (973 Program: No. 2013CB 430101), the National Natural Science Foundation of China (No. 40701130), the No-for-Profit Industry (Meteorology) Research Program, China (GYHY201106027), and Jiangsu Key Laboratory of Meteorological Observation and Information Processing (S5311026001) at the Nanjing University of Information Science and Technology, Nanjing, China.

This work was partially supported by the National Oceanic and Atmospheric Administration (NOAA), National Environmental Satellite, Data, and Information Service (NESDIS), Center for Satellite Applications and Research (STAR). The views, opinions, and findings contained in this publication are those of the authors and should not be considered an official NOAA or U.S. Government position, policy, or decision.

References

- Andersson, E., Hollingsworth, A., Kelly, G., Lönnberg, P., Pailleux, J., and Zhang, Z.: Global observing system experiments on operational statistical retrievals of satellite sounding data, *Mon. Weather Rev.*, 119, 1851–1864, 1991.
- Clerbaux, C., Boynard, A., Clarisse, L., George, M., Hadji-Lazaro, J., Herbin, H., Hurtmans, D., Pommier, M., Razavi, A., Turquety, S., Wespes, C., and Coheur, P.-F.: Monitoring of atmospheric composition using the thermal infrared IASI/MetOp sounder, *Atmos. Chem. Phys.*, 9, 6041–6054, doi:10.5194/acp-9-6041-2009, 2009.
- Collard, A. D.: Selection of IASI channels for use in numerical weather prediction, *Q. J. Roy. Meteor. Soc.*, 133, 1977–1991, 2007.
- Derber, J. C. and Wu, W.-S.: The use of TOVS cloud-cleared radiances in the NCEP SSI analysis system, *Mon. Weather Rev.*, 126, 2287–2299, 1998.
- Eyre, J.: A bias correction scheme for simulated TOVS brightness temperatures, *Tech. Memo.*, 186, ECMWF, 1992.
- Han, Y., van Delst, P., Liu, Q., Weng, F., Yan, B., Treadon, R., and Derber, J.: JCSDA Community Radiative Transfer Model (CRTM) – Version 1, NOAA Tech Report 122, 2006.
- Harris, B. and Kelly, G.: A satellite radiance bias correction scheme for data assimilation, *Q. J. Roy. Meteor. Soc.*, 127, 1453–1468, 2001.
- Kelly, G. A. and Flobert, J. F.: Radiance tuning, in: *Technical Proceedings of the Fourth International TOVS Study Conference*, Igls, Austria, 16–22 March 1988, 99–117, 1988.
- Liu, Q. and Weng, F.: Detecting the warm core of a hurricane from the Special Sensor Microwave Imager Sounder, *Geophys. Res. Lett.*, 33, L06817, doi:10.1029/2005GL025246, 2006a.
- Liu, Q. and Weng, F.: Advanced doubling–adding method for radiative transfer in planetary atmosphere, *J. Atmos. Sci.*, 63, 3459–3465, 2006b.

Impacts of AMSU-A/MHS and IASI data assimilation

Y. Bao et al.

Title Page

Abstract

Introduction

Conclusions

References

Tables

Figures



Back

Close

Full Screen / Esc

Printer-friendly Version

Interactive Discussion



Impacts of AMSU-AMHS and IASI data assimilation

Y. Bao et al.

[Title Page](#)
[Abstract](#)
[Introduction](#)
[Conclusions](#)
[References](#)
[Tables](#)
[Figures](#)




[Back](#)
[Close](#)
[Full Screen / Esc](#)
[Printer-friendly Version](#)
[Interactive Discussion](#)


Liu, Z., Schwartz, C. S., Snyder, C., and Ha, S.-Y.: Impact of assimilating AMSU-A radiances on forecasts of 2008 Atlantic tropical cyclones initialized with a limited-area ensemble Kalman filter, *Mon. Weather Rev.*, 4017–4034, 2012.

Manning, K. W. and Davis, C. A.: Verification and sensitivity experiments for the WISP95 MM5 forecasts, *Weather Forecast.*, 12, 719–735, 1997.

McMillin, L. M., Crone, L. J., and Crosby, D. S.: Adjusting satellite radiances by regression with an orthogonal transformation to a prior estimate, *J. Appl. Meteorol.*, 28, 969–975, 1989.

McNally, A. P., Derber, J. C., Wu, W., and Katz, B. B.: The use of TOVS level-1b radiances in the NCEP SSI analysis system, *Q. J. Roy. Meteor. Soc.*, 126, 689–724, 2000.

Moncet, J., Uymin, G., and Snell, H. E.: Atmospheric radiance modeling using the Optimal Spectral Sampling (OSS) method, in: Preprints, SPIE Defense and Security Symp., Conf. 5425: Algorithms and Technologies for Multispectral, Hyperspectral, and Ultraspectral Imagery X, Society of Photo-Optical Instrumentation Engineers, Orlando, FL, 5425–5437, 2004.

Nutter, P. A. and Manobianco, J.: Evaluation of the 29-km Eta Model. Part 1: Objective verification at three selected stations, *Weather Forecast.*, 14, 5–17, 1999.

Parrish, D. F. and Derber, J. C.: The National Meteorological Center's spectral statistical interpolation analysis system, *Mon. Weather Rev.*, 20, 1747–1763, 1992.

Rabier, F., Fourrié, N., Chafaï, D., and Prunet, P.: Channel selection methods for Infrared Atmospheric Sounding Interferometer radiances, *Q. J. Roy. Meteor. Soc.*, 128, 1011–1027, 2002.

Rodgers, C. D.: Information content and optimisation of high spectral resolution measurements, in: *Optical Spectroscopic Techniques and Instrumentation for Atmospheric and Space Research II*, SPIE 2380, edited by: Hays, P. B. and Wang, J., 136–147, 1996.

Rodgers, C. D.: *Inverse Methods for Atmospheres: Theory and Practice*, World Scientific, Singapore, 2000.

Uddstrom, M.: Forward model errors, Proc. 6th Int. TOVS Study Conference, Airlie, Virginia, Cooperative Institute for Meteorological Satellite Studies, Space Science and Engineering Center, University of Wisconsin, USA, 501–516, 1991.

Wan, Q. and Xu, J.: A numerical study of the rainstorm characteristics of the June 2005 flash flood with WRF/GSI data assimilation system over south-east China. *Hydrol. Process.*, 25, 1327–1341, doi:10.1002/hyp.7882, 2011.

- Weng, F.: Advances in radiative transfer modeling in support of satellite data assimilation, *J. Atmos. Sci.*, 64, 3799–3807, 2007.
- Xu, J. and Powell, A.: Dynamical downscaling precipitation over the Southwest Asian: impacts of radiance data assimilation on the hindcasts of the WRF-ARW model, *Atmos. Res.*, 111, 90–103, doi:10.1016/j.atmosres.2012.03.005, 2012.
- 5 Xu, J., Rugg, S., Byerle, L., and Liu, Z.: Weather forecasts by the WRF-ARW model with the GSI data assimilation system in the complex terrain areas of Southwest Asia, *Weather Forecast.*, 24, 987–1008, 2009.
- Zapotocny, T. H., Jung, J. A., Le Marshall, J. F., and Treadon, R. E.: A two season impact study of four satellite data types and Rawinsonde data in the NCEP global data assimilation system. *Weather Forecast.*, 23, 80–100, 2008.
- 10 Zhou, H., Gómez-Hernández, J. J., Hendricks Franssen, H.-J., and Li, L.: An approach to handling nongaussianity of parameters and state variables in ensemble kalman filtering, *Adv. Water Resour.*, 34, 844–864, doi:10.1016/j.advwatres.2011.04.014, 2011.

Impacts of AMSU-A/MHS and IASI data assimilation

Y. Bao et al.

[Title Page](#)[Abstract](#)[Introduction](#)[Conclusions](#)[References](#)[Tables](#)[Figures](#)[Back](#)[Close](#)[Full Screen / Esc](#)[Printer-friendly Version](#)[Interactive Discussion](#)

Impacts of AMSU-A/MHS and IASI data assimilation

Y. Bao et al.

Title Page

Abstract

Introduction

Conclusions

References

Tables

Figures

◀

▶

◀

▶

Back

Close

Full Screen / Esc

Printer-friendly Version

Interactive Discussion



Table 1. The experiment design includes six simulations (EXP1–EXP6).

	Experiment	Description
EXP1	CTRL	Control experiment without data assimilation
EXP2	CON	Conventional data assimilation
EXP3	MW	AMSU-A + MHS data assimilation
EXP4	IR	IASI data assimilation
EXP5	MWIR (MW + IR)	AMSU-A + MHS + IASI data assimilation
EXP6	ALL (CON + MW + IR)	Conventional + AMSU-A + MHS + IASI data assimilation

Table 2. Listed below are the 279 Channels in IASI corresponding to atmospheric temperature and humidity. The numbers indicate the order in which the channels were chosen in current data assimilation.

16	135	226	356	566	1658	2993	3248	3509	5502
38	138	230	360	571	1671	3002	3252	3518	5507
49	141	232	366	573	1786	3008	3256	3527	5509
51	144	236	371	646	1805	3014	3263	3555	5517
55	146	239	373	662	1884	3027	3281	3575	5558
57	148	243	375	668	1991	3029	3303	3577	5988
59	151	246	377	756	2019	3036	3309	3580	5992
61	154	249	379	867	2094	3047	3312	3582	5994
63	157	252	381	906	2119	3049	3322	3586	6003
66	159	254	383	921	2213	3053	3375	3589	
70	161	260	386	1027	2239	3058	3378	3599	
72	163	262	389	1046	2271	3064	3411	3653	
74	167	265	398	1121	2321	3069	3438	3658	
79	170	267	401	1133	2398	3087	3440	3661	
81	173	269	404	1191	2701	3093	3442	4032	
83	176	275	407	1194	2741	3098	3444	5368	
85	180	282	410	1271	2819	3105	3446	5371	
87	185	294	414	1479	2889	3107	3448	5379	
104	187	296	416	1509	2907	3110	3450	5381	
106	193	299	426	1513	2910	3127	3452	5383	
109	199	303	428	1521	2919	3136	3454	5397	
111	205	306	432	1536	2939	3151	3458	5399	
113	207	323	434	1574	2944	3160	3467	5401	
116	210	327	439	1579	2948	3165	3476	5403	
119	212	329	445	1585	2951	3168	3484	5405	
122	214	335	457	1587	2958	3175	3491	5455	
125	217	345	515	1626	2977	3178	3497	5480	
128	219	347	546	1639	2985	3207	3499	5483	
131	222	350	552	1643	2988	3228	3504	5485	
133	224	354	559	1652	2991	3244	3506	5492	

Impacts of AMSU-A/MHS and IASI data assimilation

Y. Bao et al.

Title Page

Abstract

Introduction

Conclusions

References

Tables

Figures



Back

Close

Full Screen / Esc

Printer-friendly Version

Interactive Discussion



Impacts of AMSU-A/MHS and IASI data assimilation

Y. Bao et al.

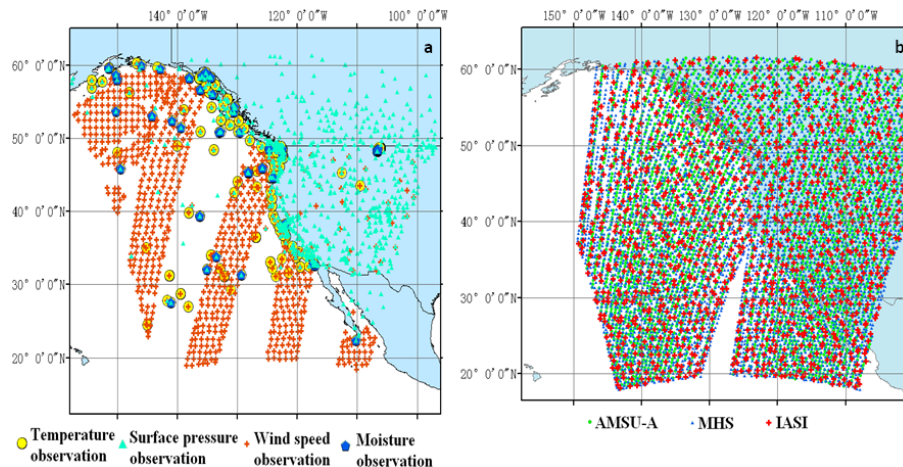


Figure 1. Distribution of observations. **(a)** conventional data on 1 July 2012 with the atmospheric temperature (yellow), moisture (dark blue) and surface pressure (light blue), wind speed (orange). **(b)** Scan coverage of AMSU-A (light blue), MHS (dark blue) and IASI (red) radiance at 18:00 UTC on 1 July 2012.

Title Page

Abstract

Introduction

Conclusions

References

Tables

Figures



Back

Close

Full Screen / Esc

Printer-friendly Version

Interactive Discussion



Impacts of AMSU-A/MHS and IASI data assimilation

Y. Bao et al.

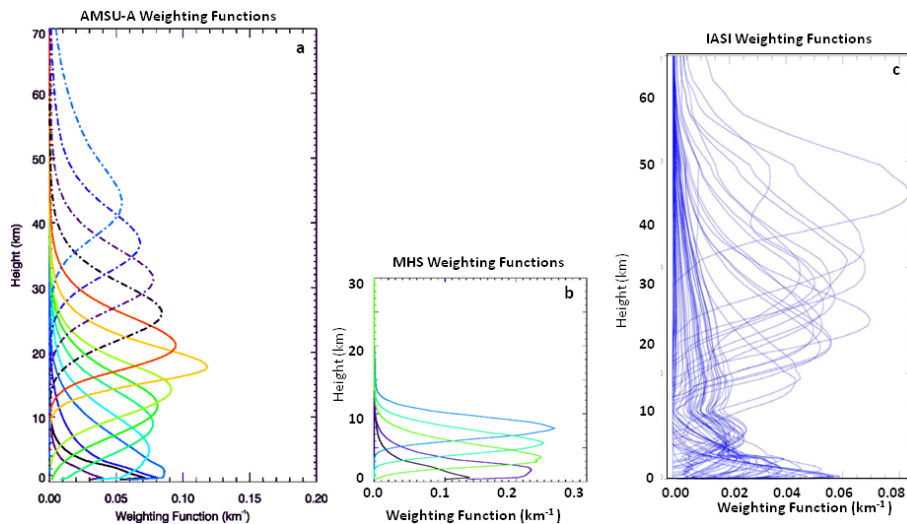


Figure 2. Vertical weighting functions for satellite observations as a function of height. **(a)** AMSUA, **(b)** MHS, **(c)** IASI.

[Title Page](#)[Abstract](#)[Introduction](#)[Conclusions](#)[References](#)[Tables](#)[Figures](#)[◀](#)[▶](#)[◀](#)[▶](#)[Back](#)[Close](#)[Full Screen / Esc](#)[Printer-friendly Version](#)[Interactive Discussion](#)

Impacts of
AMSU-A/MHS and
IASI data assimilation

Y. Bao et al.

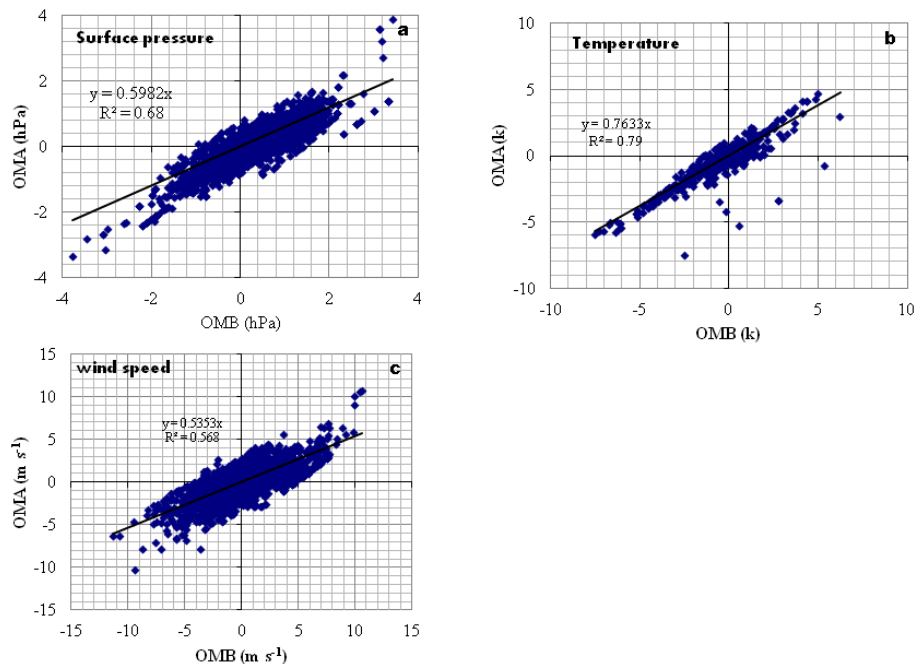


Figure 3. The scattering plot between observation minus background [OMB] and observation minus analysis [OMA] in the all data (Conventional + AMSU-A + MHS + IASI) experiment ((a) surface pressure, (b) atmospheric temperature at the height of 2 m, (c) wind speed at the height of 10 m) for 1 July 2012.

Title Page

Abstract

Introduction

Conclusions

References

Tables

Figures

◀

▶

◀

▶

Back

Close

Full Screen / Esc

Printer-friendly Version

Interactive Discussion



Impacts of AMSU-AMHS and IASI data assimilation

Y. Bao et al.

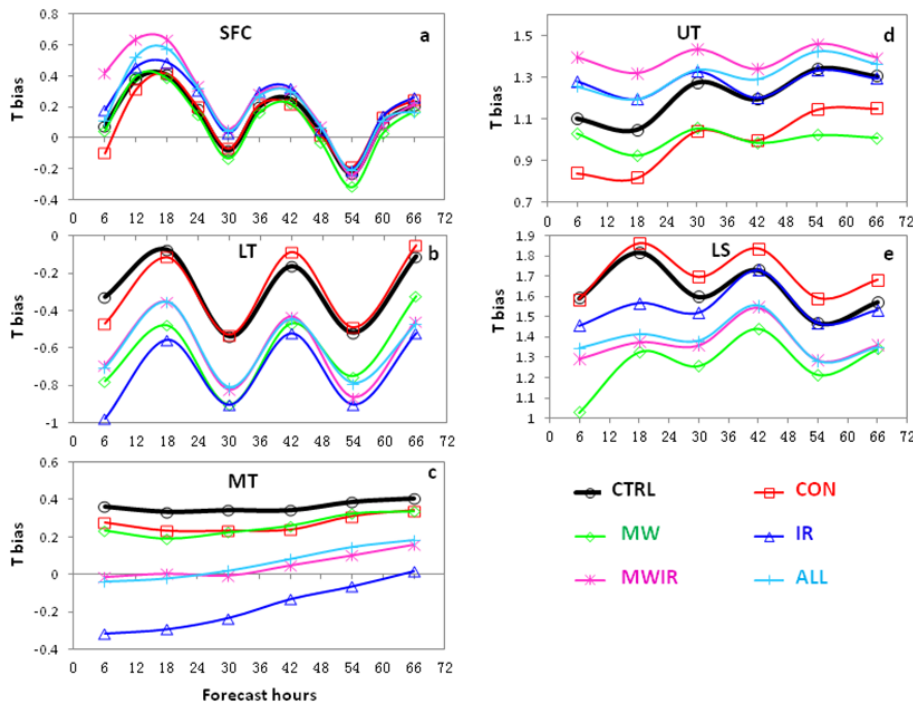


Figure 4. Bias of the temperature (T) forecasts at **(a)** surface (SFC), **(b)** lower troposphere (LT), **(c)** middle troposphere (MT), **(d)** upper troposphere (UT), **(e)** lower stratosphere (LS). Unit: $^{\circ}\text{C}$. CTRL, CON, MW, IR, MWIR and ALL are defined in Table 1.

[Title Page](#)
[Abstract](#)
[Introduction](#)
[Conclusions](#)
[References](#)
[Tables](#)
[Figures](#)

[Back](#)
[Close](#)
[Full Screen / Esc](#)
[Printer-friendly Version](#)
[Interactive Discussion](#)


Impacts of AMSU-AMHS and IASI data assimilation

Y. Bao et al.

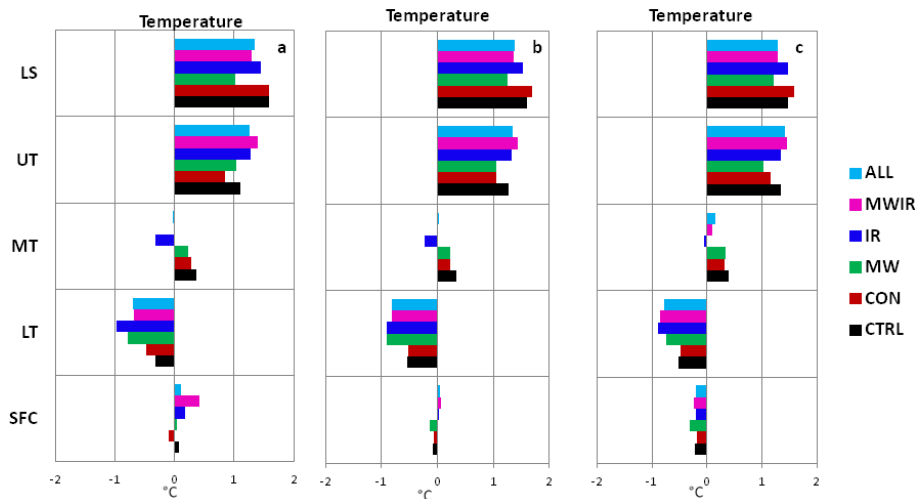


Figure 5. Bias profile of the temperature (T) forecasts at (a) 6 h, (b) 30 h, (c) 54 h forecasts. Unit: $^{\circ}\text{C}$. The other definition is same as Fig. 4.

[Title Page](#)
[Abstract](#)
[Introduction](#)
[Conclusions](#)
[References](#)
[Tables](#)
[Figures](#)
[◀](#)
[▶](#)
[◀](#)
[▶](#)
[Back](#)
[Close](#)
[Full Screen / Esc](#)
[Printer-friendly Version](#)
[Interactive Discussion](#)


Impacts of AMSU-AMHS and IASI data assimilation

Y. Bao et al.

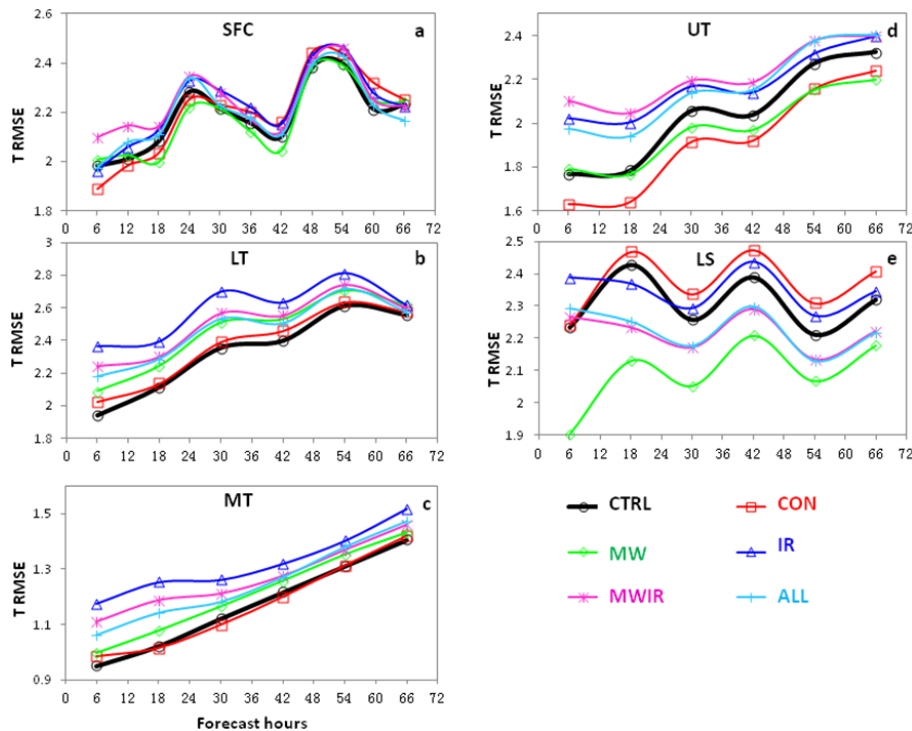


Figure 6. RMSE of the temperature (T) forecasts at (a) surface (SFC), (b) lower troposphere (LT), (c) middle troposphere (MT), (d) upper troposphere, (e) lower stratosphere. Unit: $^{\circ}\text{C}$. The other definition can be found Table 1.

Impacts of AMSU-AMHS and IASI data assimilation

Y. Bao et al.

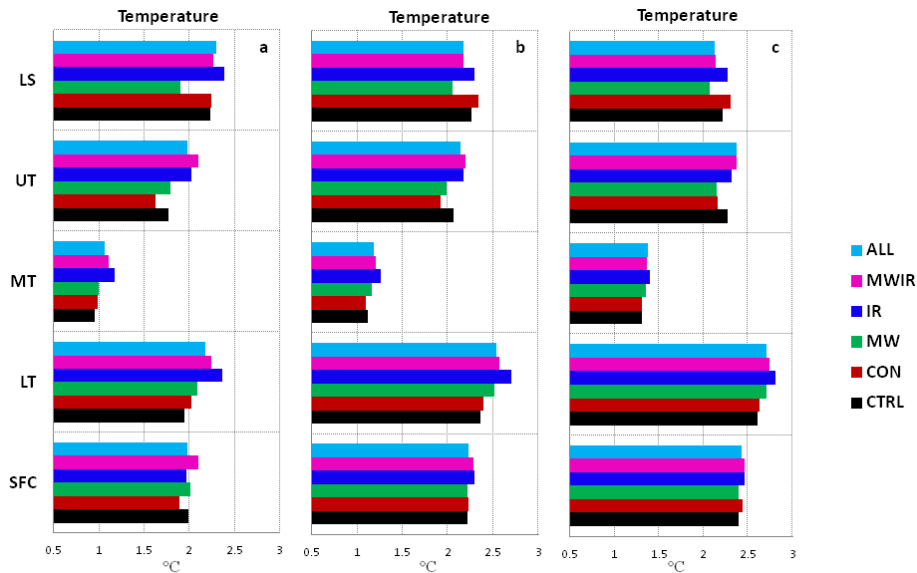


Figure 7. The RMSE profile of the temperature forecasts at (a) 6 h, (b) 30 h, (c) 54 h forecasts. Unit: $^{\circ}\text{C}$. The other definition is same as Fig. 4.

Title Page

Abstract

Introduction

Conclusions

References

Tables

Figures

◀

▶

◀

▶

Back

Close

Full Screen / Esc

Printer-friendly Version

Interactive Discussion



Impacts of AMSU-AMHS and IASI data assimilation

Y. Bao et al.

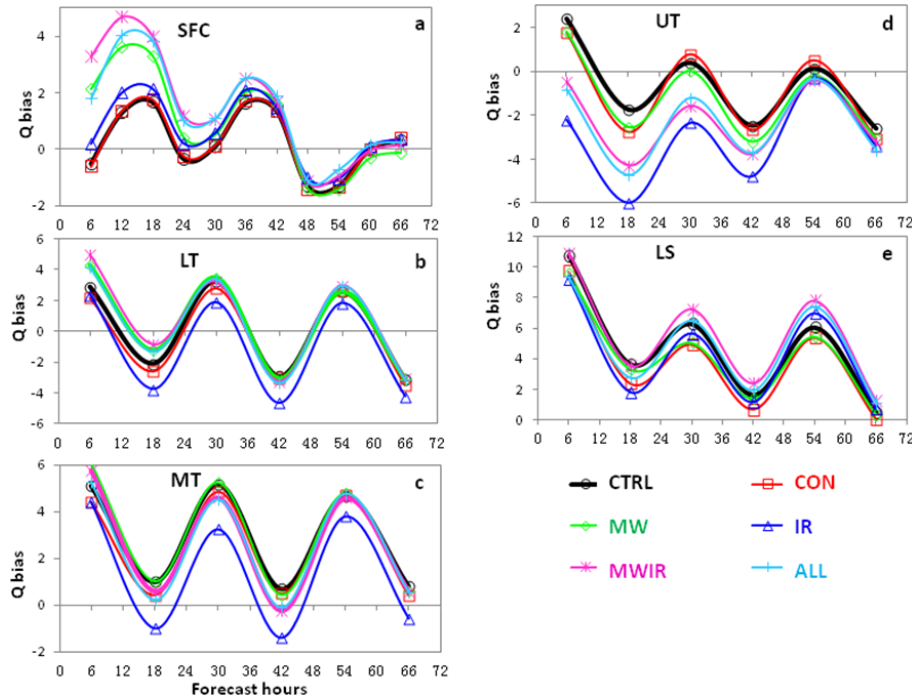


Figure 8. The bias of the specific humidity (Q) forecasts at **(a)** surface (SFC), **(b)** lower troposphere (LT), **(c)** middle troposphere (MT), **(d)** upper troposphere, **(e)** lower stratosphere. Unit: g kg^{-1} . The other definition can be found Table 1.

Title Page	
Abstract	Introduction
Conclusions	References
Tables	Figures
◀	▶
◀	▶
Back	Close
Full Screen / Esc	
Printer-friendly Version	
Interactive Discussion	



Impacts of AMSU-AMHS and IASI data assimilation

Y. Bao et al.

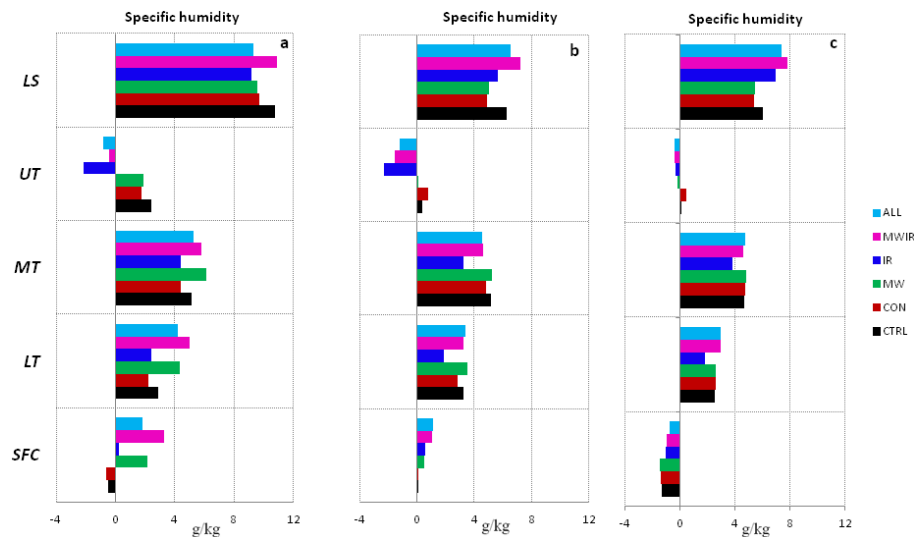


Figure 9. Bias profile of the specific humidity forecasts at **(a)** 6 h, **(b)** 30 h, **(c)** 54 h forecasts. Unit: g kg^{-1} . The other definition is same as Fig. 4.

Title Page

Abstract

Introduction

Conclusions

References

Tables

Figures

◀

▶

◀

▶

Back

Close

Full Screen / Esc

Printer-friendly Version

Interactive Discussion



Impacts of AMSU-AMHS and IASI data assimilation

Y. Bao et al.

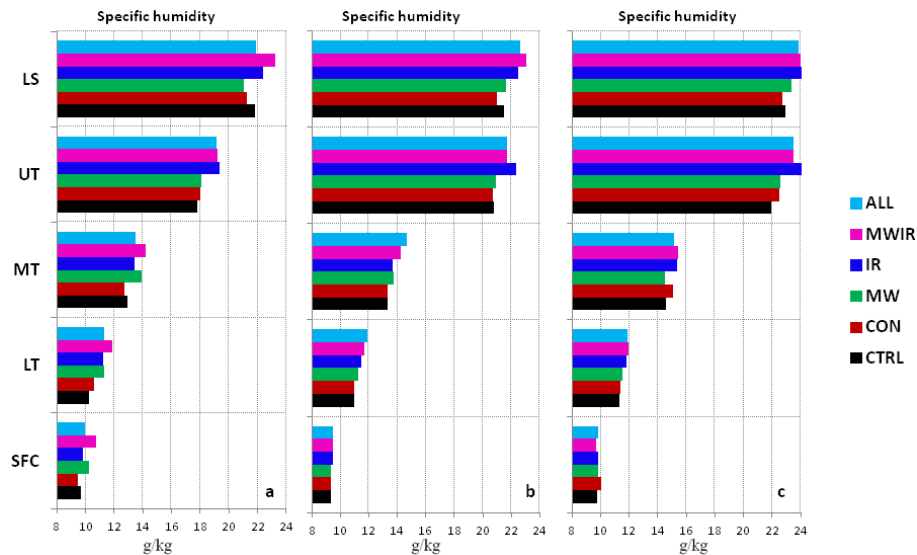


Figure 10. The RMSE profile of the specific humidity forecasts at (a) 6 h, (b) 30 h, (c) 54 h forecasts. Unit: g kg^{-1} . The other definition is same as Fig. 4.

Title Page

Abstract

Introduction

Conclusions

References

Tables

Figures

◀

▶

◀

▶

Back

Close

Full Screen / Esc

Printer-friendly Version

Interactive Discussion

